Exploring the possibilities of increasing energy density and efficiency in rechargeable batteries

Download this complimentary article collection

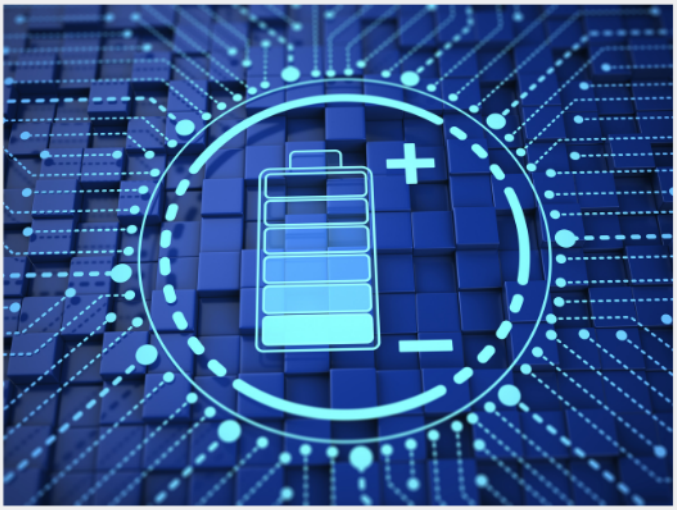

The exponential rise in the need for better, more efficient power sources has sparked an incredible amount of research into batteries. A primary focus of research has been increasing the energy density of batteries, as it allows for lighter, more portable storage of energy. Lithium-ion batteries, for example, have a much higher energy density than conventional lead-acid batteries and can be used for various purposes, such as in electric vehicles.

This article collection provides a comprehensive list of references for new methods and technologies for increasing the energy density of batteries.

Metrohm

WILEY

ADVANCED FUNCTIONAL MATERIALS
www.afm-journal.de

Check for updates

A Universal Size Design Principle for Stretchable Inorganic Electronics to Work Consistently under Different Interface Conditions

*Shuang Li, Yuqun Lan, YongAn Huang, Yuli Chen, and Yewang Su**

Stretchable inorganic electronics are usually designed and calibrated under free interface condition, while the interface conditions between the devices and skins/organs in practical applications are rather complex (free, slidable, or bonded) and may switch among them. In the ideal situation, the mechanical and electrical performances have to be consistent under different interface conditions, to ensure the accuracy and robustness of the devices. Here, the effect of interface conditions on the mechanical and electrical performances is studied for stretchable inorganic electronics with different configurations by theoretical analysis, finite element analysis and experiment. A universal size design principle is proposed for stretchable inorganic electronics to work consistently under different interface conditions, i.e., the period length of the devices/interconnects has to be the same order of magnitude as the encapsulation thickness or less. To ensure the comfort of human skin/organs, micron-scale geometrical design is necessary for epidermal electronics according to the above designed principle. This finding is of great significance for ensuring the accuracy and robustness of stretchable inorganic electronics in practical applications.

1. Introduction

Over the past decade, the rapidly developing technology of stretchable inorganic electronics[1–3] has made a large number of functional devices with broad interest and potential for impact (e.g., stretchable battery,[4] sensors for monitoring heart activity,[5] stretchable light emitting diodes,[6,7] optogenetic platforms,[8] and strain sensors[9]) applied to complex interfaces such as human skins and organ surfaces. Mechanically guided structural designs are usually exploited to integrate conventional hard inorganic semiconductor components and geometrically structural interconnects onto soft substrates (**Figure 1**a), which guarantee that the electronic systems can undergo large deformations without failure.[3,10] Up to now, various strategies based on wavy,[11–13] island-bridge[4,7,14–16] (e.g., arc-shaped interconnects,[17–20] serpentine interconnects,[7,21–26] 2D spiral interconnects,[27–31] and 3D helical interconnects[32–35]), fractal,[4,25,36–41] kirigami structures,[42–48] etc. have been adopted in the state-of-the-art stretchable inorganic electronics. The stretchability has developed from >10% of the earliest wavy structure[11,12] to 60% of the serpentine interconnects, and even to greater than 100% for the 3D helical interconnects.[32]

The accuracy and the robustness of the performances of stretchable electronics are critically important for large-scale commercial use to improve people's medical conditions and quality of life. On this topic, we point out a common and vital problem with the stretchable wristband as an example, as shown in Figure 1a. Such devices are usually designed and calibrated under free interface condition, but the interface conditions between the devices and skins/organs in practical applications are rather complex (free, slidable or bonded) and may switch among them (Figure 1b, details shown in Note S1, Supporting Information). The actual deformation mode and strain distribution may be different from those of the initial design target and calibrated result under the free interface condition, which could further lead to the change and unrobustness of the electrical performance and even fracture after long-term fatigue. We show the difference of the strain distribution by an example of a serpentine network architecture bonded on the soft substrate with typical parameters (details shown in the Experimental Section and Figure S1, Supporting Information; additional discussion for the effect of Young's modulus of human skin shown in Note S2, Supporting Information). The finite element analysis (FEA) demonstrates that the maximum principal strain in the network, which is subject to 20%

S. Li, Y. Lan, Y. Su
State Key Laboratory of Nonlinear Mechanics
Institute of Mechanics
Chinese Academy of Sciences
Beijing 100190, China
E-mail: yewangsu@imech.ac.cn

S. Li, Y. Lan, Y. Su
School of Engineering Science
University of Chinese Academy of Sciences
Beijing 100049, China

Y. Huang
State Key Lab Digital Manufacturing Equipment and Technology, and Flexible Electronics Research Center
Huazhong University of Science and Technology
Wuhan, Hubei 430074, China

Y. Chen
Institute of Solid Mechanics
Beihang University (BUAA)
Beijing 100191, China

The ORCID identification number(s) for the author(s) of this article can be found under https://doi.org/10.1002/adfm.202210880.

DOI: 10.1002/adfm.202210880

 © 2022 Wiley-VCH GmbH

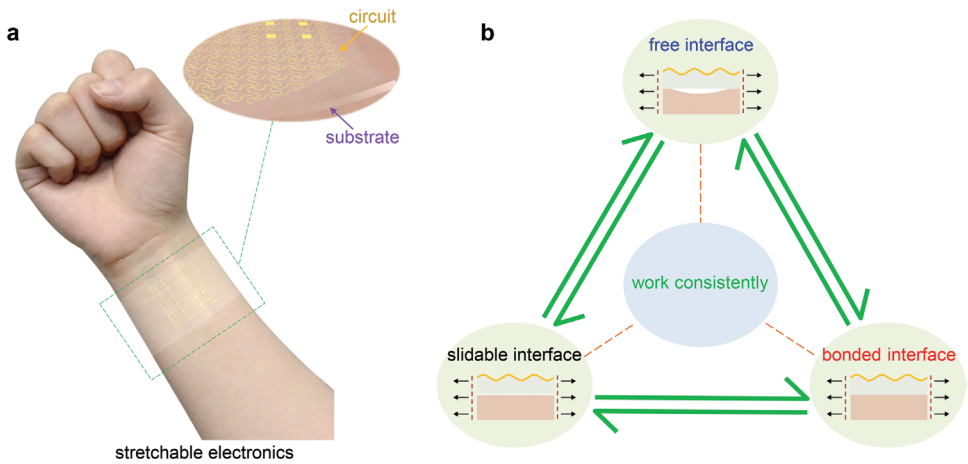

Figure 1. Stretchable inorganic electronics under different interface conditions. a) Schematic diagram of a stretchable wristband as an example. b) The requirement of working consistently under complex interface conditions (free, slidable, or bonded) between the devices and skins/organs in practical applications.

uniaxial applied strain under different interface conditions, can be quite different (relative difference ≈50%), which indicates that the stretchability changes with the switch of interface conditions. Such an effect can greatly limit the practical use and further commercialization of the devices. In the ideal situation, the mechanical and electrical performances (e.g., stretchability, durability, conductivity, and sensing performance) should be consistent under different interface conditions, so as to ensure that the devices can work accurately and robustly not only in the theoretical/FEA models and calibration tests under free interface condition in the laboratory, but also under the complex mechanical conditions on the surfaces of human skins or other organs. Is there any universal design principle for stretchable inorganic electronics to achieve this target?

In this paper, the effect of interface conditions on the mechanical and electrical performances is investigated for stretchable inorganic electronics with different configurations. To reveal the law theoretically, the wavy structure is studied first to show the relationship between the mechanical performances and the ratio of the encapsulation thickness to the period length of the devices/interconnects under different interface conditions. For the stretchable inorganic devices/interconnects with different configurations, a universal qualitative analysis according to superposition principle[49] and Saint-Venant's principle[50–52] is conducted, which gives the similar conclusions as the wavy structure. On this basis, a universal and simple size design principle is proposed for stretchable inorganic electronics to work consistently under different interface conditions. The adaptability of the design principle is verified by the FEA and the experiment on the serpentine-structure stretchable electronics as an example.

2. Results and Discussion

2.1. Analysis of the Wavy-Structure Stretchable Electronics

In order to investigate the problem theoretically, the wavy structure bonded on soft substrate without any prestrain or prestress, the configuration of which is similar to the pioneer structure of stretchable electronics formed by release of the prestrain of the substrate,[11,12] is adopted as shown in **Figure 2**a, without loss of generality. The initial configuration of the wavy structure is given as $w_0 = A_0\cos(k_0x_1)$, where A_0 is the initial amplitude and k_0 is the initial wave number; $\lambda_0 = 2\pi/k_0$ is the initial period length. For the uniaxial applied strain of ε_{app}, the maximum principal strain $\varepsilon_{\max}$ in the wavy structure bonded on the soft substrate, which is under the free, slidable and bonded interface conditions between the bottom surface and the skin, respectively, can be approximately obtained theoretically by drawing lessons from the buckling theory of the film/substrate systems,[53–58] especially the works developed by Suo et al.,[55] Gao et al.,[57] and Feng et al.[56] (details shown in Note S3, Supporting Information). Here, the skin is treated as a rigid board, since its modulus is two orders of magnitude larger than that of the soft substrate. The maximum principal strain $\varepsilon_{\max}$ in the stretching state changes with the applied strain ε_{app} as

$$\varepsilon_{\max} = hk_0^2\frac{A_0\left(1+\varepsilon_{\text{app}}\right)^2 - A}{2\left(1+\varepsilon_{\text{app}}\right)^2} + \frac{\left(\pi/2-1\right)\overline{E}_s hg\left(k_0H\right)\left(A_0-A\right)}{2\overline{EI}k_0} \tag{1}$$

where $\overline{EI} = \overline{E}_{\text{PI}}h^3/12$ is bending stiffness of the wavy structure, $\overline{E}_{\text{PI}} = E_{\text{PI}}/(1-\nu_{\text{PI}}^2)$ the effective Young's modulus, ν_{PI} the Poisson's ratio, and h the thickness; $\overline{E}_s = E_s/(1-\nu_s^2)$ is the effective Young's modulus of the soft substrate, H the thickness, E_s Young's modulus, and ν_s Poisson's ratio. In Equation (1), the instant amplitude A can be obtained by the following equation containing the elliptic integral of the second kind $Elliptic E()$,

$$\sqrt{\frac{A^2k_0^2+\left(1+\varepsilon_{app}\right)^2}{A_0^2k_0^2+1}}\,Elliptic\,E\left[1/\sqrt{1+\left(1+\varepsilon_{\text{app}}\right)^2/\left(A^2k_0^2\right)}\right] = Elliptic\,E\left[1/\sqrt{1+1/\left(A_0^2k_0^2\right)}\right] \tag{2}$$

and the dimensionless parameter of $g(k_0H)$ for bonded, slidable and free interface conditions are given by Suo et al.,[55] Gao et al.[57] and Feng et al.,[56] respectively,

© 2022 Wiley-VCH GmbH

16163028, 2023, 7, Downloaded from https://onlinelibrary.wiley.com/doi/10.1002/adfm.202210880 by Institute Of Mechanics (Cas), Wiley Online Library on [08/05/2023]. See the Terms and Conditions (https://onlinelibrary.wiley.com/terms-and-conditions) on Wiley Online Library for rules of use; OA articles are governed by the applicable Creative Commons License

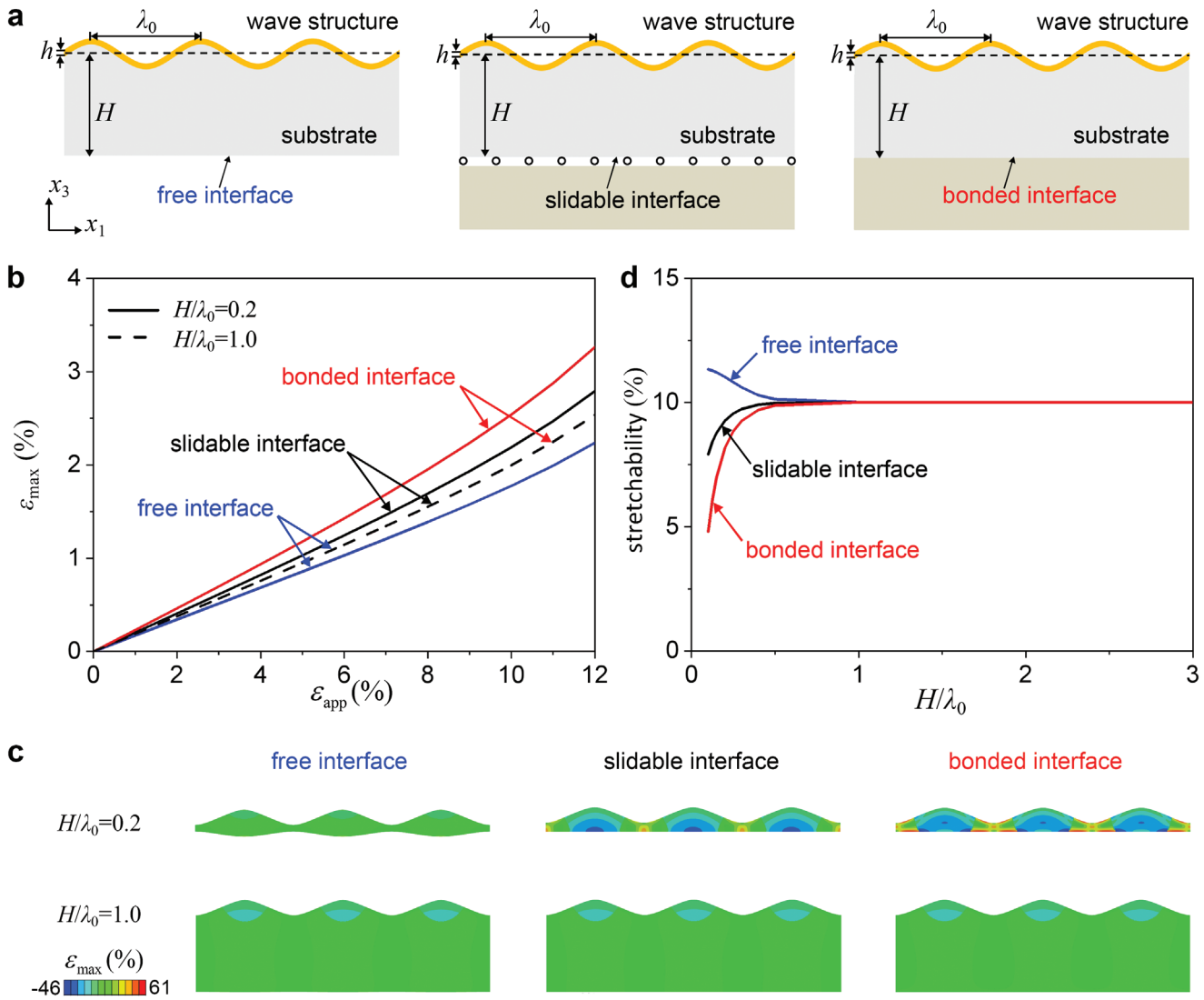

Figure 2. Analysis of the wavy-structure stretchable electronics under different interface conditions. a) Three interface conditions of wavy-structure stretchable electronics (free, slidable, and bonded). b) Curves of maximum principal strain versus applied strain of wavy-structure stretchable electronics under three interface conditions. c) Strain distribution of wavy-structure stretchable electronics with thin/thick encapsulation under three interface conditions by the FEA. d) Curves of stretchability of wavy-structure stretchable electronics versus the ratio of the encapsulation thickness to the period length under three interface conditions.

$$g(k_0H)=\begin{cases}\dfrac{(3-4\nu_s)\cosh(2k_0H)+5-12\nu_s+8\nu_s^2+2(k_0H)^2}{(6-8\nu_s)\sinh(2k_0H)-4k_0H} & \text{for bonded,}\\[2ex] \dfrac{2k_0H+\sinh(2k_0H)}{4\sinh^2(k_0H)} & \text{for slidable,}\\[2ex] \dfrac{\sinh^2(k_0H)-(k_0H)^2}{\sinh(2k_0H)+2k_0H} & \text{for free}\end{cases} \quad (3)$$

Here, $g(k_0H)$ monotonically decreases with k_0H for the bonded and slidable interface conditions, while it monotonically increases with k_0H for the free interface condition.

Taking the initial period length $\lambda_0 = 80h$, the initial amplitude $A_0 = 10h$ and the modulus ratio $\overline{E}_{PI}/\overline{E}_s = 3.45 \times 10^4$, Figure 2b shows the changes of the maximum principal strain of the wavy structure with the applied strain under three interface conditions (free, slidable, and bonded) according to Equation (1). It is found that, for the large period length (H/λ_0= 0.2), the maximum principal strain ε_{max} in the wavy structure subjected to the same applied strain under the three interface conditions is quite different, and the maximum principal strain under bonded interface condition is ≈30% larger than that under free interface condition; while for the small period length (H/λ_0= 1), the maximum principal strain in the wavy structure subjected to the same applied strain under the three interface conditions approaches almost the same and only slightly larger than that of the large period length under free interface condition. The corresponding FEA results also directly reflect the different deformation of the encapsulation under the three interface conditions (Figure 2c). For the given maximum principal strain ε_{max} = 2%, Figure 2d shows the curves of the stretchability of the wavy structure versus the ratio of the encapsulation thickness to the period length under the three interface conditions

© 2022 Wiley-VCH GmbH

16163028, 2023, 7, Downloaded from https://onlinelibrary.wiley.com/doi/10.1002/adfm.202210880 by Institute Of Mechanics (Cas), Wiley Online Library on [08/05/2023]. See the Terms and Conditions (https://onlinelibrary.wiley.com/terms-and-conditions) on Wiley Online Library for rules of use; OA articles are governed by the applicable Creative Commons License

according to Equation (1). It is found that: i) the stretchability increases with the increase of the ratio of the encapsulation thickness to the period length under the bonded interface condition, which is contrary to the free interface condition; ii) the stretchability under different interface conditions is quite different for the large period length (thin encapsulation), while, under these conditions, it tends to be the same value when the encapsulation thickness reaches the period length of the wavy structure. This suggests that the relatively small period length (thick encapsulation) is helpful to ensure the accuracy and the robustness of the performances of stretchable inorganic electronics in practical applications, in spite of the interface condition. The key mechanism can be understood as follows. The encapsulation constrains the deformation of the wavy structure and thus increases the maximum principal strain under a given applied strain. Such constraint becomes stronger for larger encapsulation thickness under the free interface condition or for smaller encapsulation thickness under the slidable/bonded interface conditions. When the encapsulation thickness is thick enough, the interface conditions on the bottom surface have a negligible effect on the wavy structure, and thus the constraint approaches the same degree. Therefore, the mechanical performances under different interface conditions are quite different for the large period length (thin encapsulation), while they tend to be the same for the small period length (thick encapsulation).

For the wavy structure with both the top and the bottom encapsulation (thickness of H for each layer), Equation (1) can also be used to calculate the stretchability as long as g is replaced with g', which is equal to $2g_{\text{free}}$ for the free interface condition, or equal to $g_{\text{free}} + g_{\text{slidable}}$ for the slidable interface condition, or equal to $g_{\text{free}} + g_{\text{bonded}}$ for the bonded interface condition, considering that the top side is always the free interface condition (details shown in Note S3, Supporting Information). Figure S5 (Supporting Information) shows the curves of stretchability of the wavy-structure stretchable electronics encapsulated from both the top and the bottom versus the ratio of the encapsulation thickness to the period length under three interface conditions. Note that the trend of the stretchability under free interface condition is opposite to that of the other two interface conditions for single-side encapsulation. Therefore, for the wavy structure with both the top and the bottom encapsulation, when g_{free} and g_{slidable} or g_{bonded} are superposed, a slight non-monotonous of the stretchability could occur. However, this does not affect the trend of the stretchability similar to that of the single-side encapsulation on the whole and also the size design principle. Besides the wavy structure, do the stretchable inorganic electronics with other configurations have the similar conclusion?

2.2. Universal Size Design Principle for Stretchable Inorganic Electronics

In general, despite the different configurations, the stretchable inorganic devices/interconnects have the characteristics of periodicity and symmetry, and thus a qualitative analysis according to superposition principle[49] and Saint–Venant's principle[50–52] can be conducted on one period of the devices/interconnects, which gives the similar conclusion as the wavy

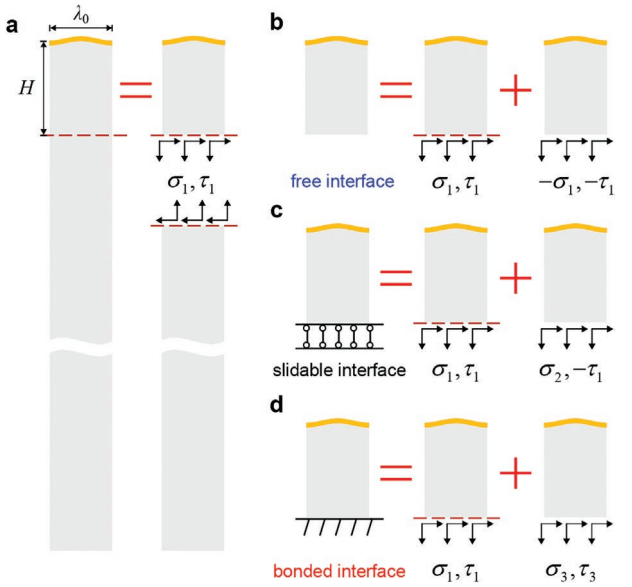

Figure 3. Universal stress analysis of stretchable inorganic electronics. a) Stretchable electronics with infinite encapsulation thickness. Stress decomposition of encapsulated stretchable electronics under b) free, c) slidable, and d) bonded interface conditions.

structure. Here, the stretchable electronics are considered as linear elastic solids without loss of generality. As the basis for subsequent analysis, we first suppose a stretchable inorganic device/interconnect with the period length λ_0 and infinite encapsulation thickness. Owing to the periodicity, only one period is taken out for the analysis, as shown in the left subgraph of **Figure 3**a. It can be divided into two parts: one part with thickness H and the rest, with the normal stress σ_1 and shear stress τ_1 acting on the parting planes and the horizontal stretching displacement boundary on the two sides (right subgraph of Figure 3a). Let V_H denote the volume of the encapsulation between the section $x_3 = H$ and $x_3 = \infty$, and $E(H)$ denote the strain energy in V_H. Noted that the "strain energy" mentioned here is calculated by the stresses and strains excluding the elastic field of homogeneously stretching in the encapsulation material, and it is actually caused by the influence of the inhomogeneous deformation of the device/interconnect. The exponential attenuation law of strain energy in Saint–Venant's principle[50–52] gives

$$E(H) \leq E(0)e^{(-2\alpha H)} \tag{4}$$

where α is a coefficient related to λ_0. Although the estimates of α are various for different boundary-value problems, they are typically on the order of $1/\lambda_0$.[50] Thus, the strain/stress increment in the encapsulation should also decay exponentially with H/λ_0. For the elastic fields of the actual stretchable inorganic device/interconnect with the finite encapsulation thickness H under the free interface condition (left subgraph of Figure 3b), the slidable interface condition (left subgraph of Figure 3c) and the bonded interface condition (left subgraph of Figure 3d), they can be divided into two elastic fields by using superposition principle[49] respectively: one with the normal stress σ_1 and shear stress τ_1 in the bottom interface, the other with the

© 2022 Wiley-VCH GmbH

16163028, 2023, 7, Downloaded from https://onlinelibrary.wiley.com/doi/10.1002/adfm.202210880 by Institute Of Mechanics (Cas), Wiley Online Library on [08/05/2023]. See the Terms and Conditions (https://onlinelibrary.wiley.com/terms-and-conditions) on Wiley Online Library for rules of use; OA articles are governed by the applicable Creative Commons License

normal stress – σ_1, σ_2 or σ_3 and shear stress – τ_1, – τ_1 or τ_3 in the bottom interface (right subgraphs of Figure 3b–d). The effect on the strain of the device caused by the former one is the same as the case of infinite encapsulation thickness, and the effect caused by the latter one decreases with the increase of encapsulation thickness H. In order to facilitate the general understanding of the rate of the energy attenuation, we suppose a typical value $\alpha = 1/\lambda_0$ in Equation (4) as an example, which yields $E(H) \leq E(0)e^{(-2H/\lambda_0)}$. When $H/\lambda_0 = 1$ and $H/\lambda_0 = 2$, $E(H)/E(0) \leq 13.5\%$ and $E(H)/E(0) \leq 1.8\%$ are obtained, respectively, which indicates that the effect caused by the interface condition could be neglected when H/λ_0 is on the order of magnitude of 1 ($H/\lambda_0 \sim 1$). Therefore, when

$$H/\lambda_0 \sim 1 \tag{5}$$

or more, the strain distribution of the device under different interface conditions finally approaches a same stable value. Generally, the superposition principle is applied to linear elasticity. In the practical applications of the stretchable electronics, the nonlinear behaviors usually exist and thus the real strain distribution is different from the analysis under the assumption of small deformation. In this work, in order to obtain a general rule theoretically, we adopt the assumption of small deformation considering that it is impossible to accurately solve each complex stretchable configuration with the encapsulation. Noted that the qualitative analysis finally gives an order of magnitude estimate, and it will not fail due to a few of strain/stress differences. All of the finite element analyses in this work are without the assumption of small deformation, which can also prove the validity of the size design principle. The following is a typical case where the superposition principle will fail even when it is only used to estimate the order of magnitude: when the stretchable electronics are stretched greatly (e.g., 400%: λ_0–$5\lambda_0$), the encapsulation thickness becomes very small (H–$0.45H$) due to Poisson's ratio effect, and λ/H becomes more than 10 times of the original, thus the initial design is no longer valid. For the stretchable interconnects with fractal design that have different period lengths in different orders, the maximum period length should be used in the size design principle. As shown in Figure S6 (Supporting Information), as long as $H/\lambda_3 \sim 1$ is satisfied, $H/\lambda_2 > 1$ and $H/\lambda_1 \gg 1$ are automatically satisfied. Therefore, the stretchable interconnects can work consistently under different interface conditions. For the stretchable inorganic electronics with different configurations encapsulated from both the top and the bottom, such qualitative analysis can also be conducted on one period of the devices/interconnects, as shown in Figure S7 (Supporting Information). The top encapsulation and the bottom encapsulation can be decomposed separately, and then the effect on the devices/interconnects can be summed. Similar to the wave structure encapsulated from both the top and the bottom, there could be slight non-monotonous of the stretchability. However, this does not affect the trend of the stretchability similar to that of the single-side encapsulation on the whole and also the size design principle.

On the basis of above results, a universal and simple size design principle for stretchable inorganic electronics to work consistently under different interface conditions can be proposed, that is, the period length of the devices/interconnects should be the same order of magnitude as the encapsulation thickness or less such that the mechanical and electrical performances (e.g., stretchability, durability, conductivity and sensing performance) are no longer sensitive to different interfaces. Then other geometric and material parameters should be optimized on this basis. Considering requirement of the comfort of the human skin/organs, the thickness of the encapsulation layer of the epidermal electronics should preferably not exceed 100 μm, which means that the period length of the devices/interconnects is better on the order of 100 μm or smaller. From this point of view, micron-scale geometrical design is necessary for epidermal electronics according to above design principle. This finding is of much significance since the design of the ratio of the encapsulation thickness to the period length of the devices/interconnects has not been seriously considered but only prepared randomly in general. It provides theoretical guidance for ensuring the accuracy and the robustness of the mechanical and electrical performances of stretchable inorganic electronics in practical applications.

On the other hand, this work expands the understanding of the role of the solid encapsulation. The solid encapsulation is essential in most practical applications, not only to physically protect the circuits and the surrounding tissues/organs from damage by scratch or leakage of electricity, but also to avoid the failure of functional components due to the chemical reactions that can follow upon contact with sweat or body fluid. However, in the conventional wisdom the solid encapsulation strategies generally cause a reduction in the stretchability, as compared to the unencapsulated inorganic electronics.[3,21] Therefore, relatively thin encapsulation was usually adopted in the stretchable inorganic electronics.[21] Here, we point out that the relatively thick encapsulation is beneficial to the accuracy and the robustness of the mechanical and electrical performances of stretchable inorganic electronics under different interface conditions.

2.3. Verification of the Size Design Principle by an Example of the Serpentine Structure

Serpentine structure is the most popular configuration in the design of the stretchable inorganic electronics nowadays because of the excellent stretchability.[7] In order to verify the adaptability of the size design principle, we studied the relationship between the mechanical and electrical performances of the serpentine-structure stretchable electronics and encapsulation thickness under different interface conditions (free, slidable, and bonded, **Figure 4**a) by the FEA and experiment, as an example. The serpentine structure is inside the encapsulation with a thickness of $2H$ and at the middle plane along the thickness direction. For the thickness h= 0.2 mm, the width w_{PI}= 0.2 mm, the radius R= 0.8 mm, the period length $\lambda_0 = 4R$, the length L= 4 mm and the given maximum principal strain ε_{max} = 0.6% of the serpentine structure (detailed layout shown in Figure S8, Supporting Information), Figure 4b shows the curves of the stretchability of the serpentine structure versus the ratio of the encapsulation thickness to the period length under the three interface conditions by FEA. It is also found that: i) on the whole, the stretchability increases with the increase of the ratio of the encapsulation thickness to

© 2022 Wiley-VCH GmbH

16163028, 2023, 7, Downloaded from https://onlinelibrary.wiley.com/doi/10.1002/adfm.202210880 by Institute Of Mechanics (Cas), Wiley Online Library on [08/05/2023]. See the Terms and Conditions (https://onlinelibrary.wiley.com/terms-and-conditions) on Wiley Online Library for rules of use; OA articles are governed by the applicable Creative Commons License

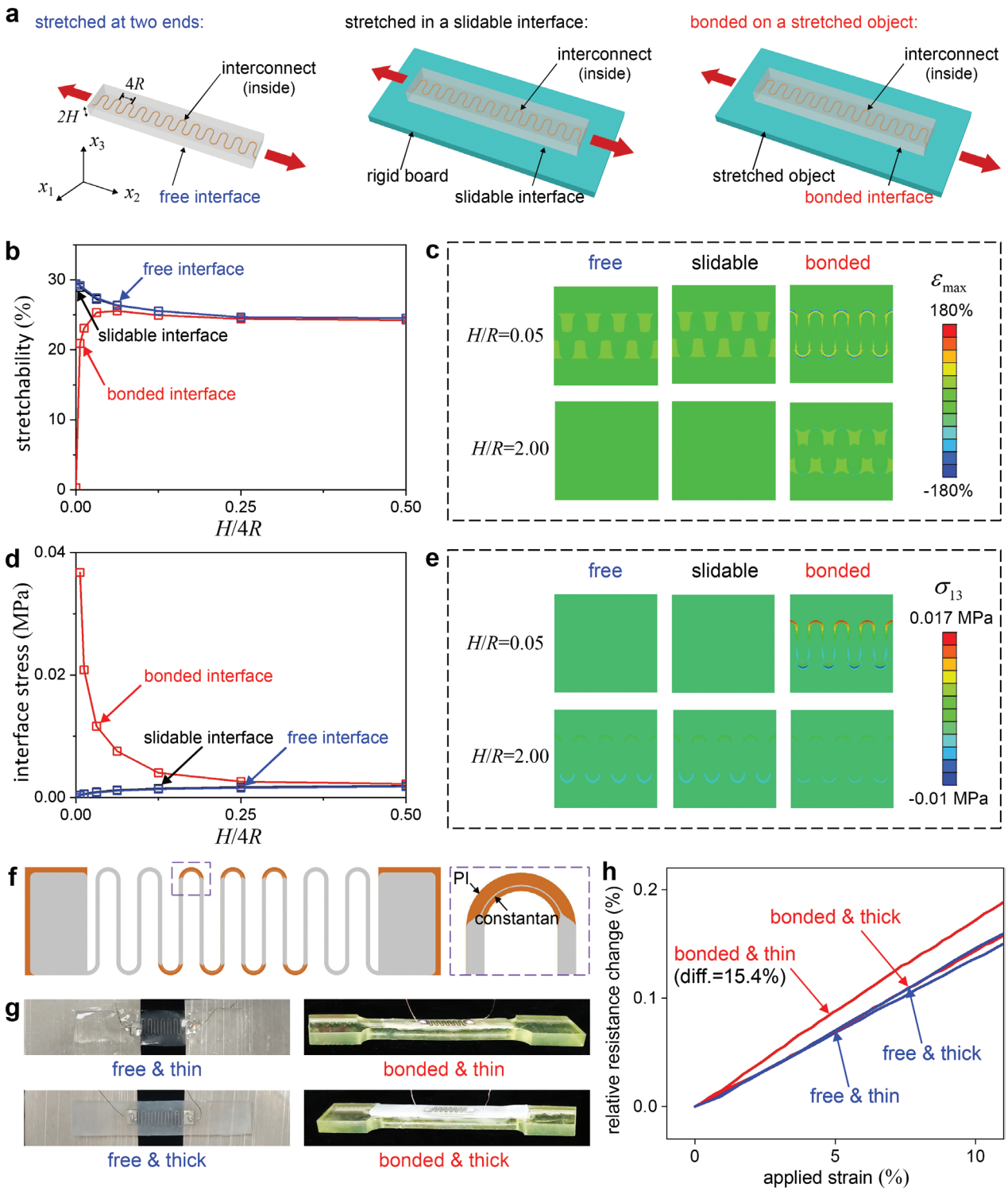

Figure 4. Verification of the size design principle by an example of the serpentine-structure stretchable electronics. a) Three interface conditions for serpentine-structure stretchable electronics (free, slidable, and bonded). b) Curves of stretchability of serpentine-structure stretchable electronics versus the ratio of the encapsulation thickness to the period length under three interface conditions. c) Strain distribution of the encapsulation of the serpentine-structure stretchable electronics with thin/thick encapsulation under three interface conditions by the FEA. d) Curves of the maximum interface stress (shear stress σ_{13}) between the serpentine structure and the encapsulation versus the ratio of the encapsulation thickness to the period length under three interface conditions. e) Distribution of interface stress (shear stress σ_{13}) between the serpentine structure and the encapsulation under three interface conditions by the FEA. f) Layout of the serpentine structure with off-axis constantan foil. g) Tensile samples of the serpentine structure with thin/thick encapsulation under free interface and bonded interface conditions. h) Curves of relative resistance change versus applied strain of the serpentine structure with thin/thick encapsulation under free interface and bonded interface conditions.

© 2022 Wiley-VCH GmbH

16163028, 2023, 7, Downloaded from https://onlinelibrary.wiley.com/doi/10.1002/adfm.202210880 by Institute Of Mechanics (Cas), Wiley Online Library on [08/05/2023]. See the Terms and Conditions (https://onlinelibrary.wiley.com/terms-and-conditions) on Wiley Online Library for rules of use; OA articles are governed by the applicable Creative Commons License

the period length under the bonded interface condition, which is contrary to the free interface condition; ii) the stretchability under different interface conditions is quite different for the large period length, while, under these conditions, it tends to be the same value when the encapsulation thickness reaches the period length of the serpentine structure, i.e., H/λ_0~1, which conforms to the order of magnitude estimation in Equation (4). The corresponding FEA results directly reflect the different deformation of the encapsulation under the three interface conditions (Figure 4c). To ensure the good bonding between the inorganic structure and the encapsulation, the interface stress between the inorganic structure and the encapsulation should be reduced as much as possible, so that it is less than the maximum bonding strength that the two materials can withstand. In fact, the size design principle in this work can also help reduce the interface stress between the inorganic structure and the encapsulation. Figure 4d shows the curves of the maximum interface stress (shear stress σ_{13}) between the serpentine structure and the encapsulation versus the ratio of the encapsulation thickness to the period length under the three interface conditions by FEA. It is found that: i) the maximum interface stress decreases with the increase of the ratio of the encapsulation thickness to the period length under the bonded interface condition, which is contrary to the free interface condition; ii) the maximum interface stress under different interface conditions is quite different for the large period length, while, under these conditions, it tends to be the same value when the encapsulation thickness reaches the period length of the serpentine structure, i.e., $H/\lambda_0 \sim 1$. Figure 4e directly reflects the different interface stress distribution under the three interface conditions. The maximum interface stress (shear stress σ_{13}) between the inorganic structure and the encapsulation reaches 0.017 MPa for $H/R = 0.05$ under the bonded interface condition, while it is only 0.002 MPa for $H/R = 2.00$ under the three interface conditions.

Besides, we designed an experiment to verify the difference of the maximum principal strain of the serpentine structure with thin/thick encapsulation (equivalent to large/small period length) under different interface conditions. Since the maximum principal strain occurs in the arc segments, several thin constantan foils are set off-axis in the arc segments of the serpentine structure to reflect the strain level by the resistance change. The parameters of the PI serpentine structure are the same as the FEA model in Figure 4b, and the width w_{con}= 25 µm, the thickness h_{con}= 4 µm, the distance d= 50 µm from the inner edge of the constantan foil to the central axis of PI layer, and the Young's modulus E_{con}= 163 GPa are for the constantan foils (Figure 4f; Figure S9, Supporting Information). The fabrication process is shown in the Experimental Section. Figure 4g exhibits the tensile samples of the serpentine structure with thin/thick (0.25 mm / 0.8 mm) encapsulation (Ecoflex 00–30, Smooth-On, USA) for the free interface condition and the bonded interface condition, respectively. The serpentine structure is inside the encapsulation, just like the diagram in Figure 4a. Figure 4h shows the curves of the relative resistance changes versus the applied strain of the serpentine structure with thin/thick encapsulation under the free/bonded interface conditions. For the thin encapsulation, the relative resistance changes under the free/bonded interface conditions have a difference of 15.4%, while for the thick encapsulation, the relative resistance changes under the free/bonded interface conditions are almost the same. Another set of repeated experiment shows the same conclusion with 14.1% difference of the relative resistance changes under the free/bonded interface conditions for the thin encapsulation (Figure S10, Supporting Information). Considering the linear relationship between the relative resistance change and the maximum principal strain, these curves verify the nonnegligible difference of the maximum principal strain of the serpentine structure for thin encapsulation under different interface conditions and prove the consistency for thick encapsulation.

The functions and geometrical configurations of stretchable inorganic electronics are diverse, and thus the final design needs to consider various requirements. The appropriate stiffness (rigidity) is one of the important requirements in the practical applications, which is related to both of the material parameters and the geometric configurations. For example, the tensile stiffness of the serpentine structure is related to the thickness h, the width w, the radius R, the length L, Young's modulus E, and Poisson's ratio ν.[23–25] The size design principle proposed in this work requires that the period length of the serpentine structure is the same order of magnitude as the encapsulation thickness or less. Therefore, only the value range of the radius R is limited. On this basis, the tensile stiffness can be further optimized according to previous researches.[23–25] Our work does not give all the design principles, but gives one important and general design principle, which has not been found before.

3. Conclusion

The rapidly developing stretchable inorganic electronic technology has proved that "they can do a lot" over the past decade, but at this stage, "how they can do accurately and robustly" should be discussed on the table. On the basis of the study of the effect of interface conditions on the mechanical and electrical performances for stretchable inorganic electronics with different configurations, this paper gives a simple and universal size design principle for stretchable inorganic electronics to work consistently under different interface conditions, i.e., the period length of the devices/interconnects should be the same order of magnitude as the encapsulation thickness or less. It also provides an additional beneficial effect on reducing the interface stress to ensure the good bonding between the inorganic structure and the encapsulation, which helps to improve the robustness of the devices. To ensure the comfort of human skin/organs, micron-scale geometrical design is necessary for epidermal electronics according to above design principle.

4. Experimental Section

Typical Parameters of the Serpentine Network Architecture: In Figure S1 (Supporting Information), the difference of the strain distribution was shown by an example of a serpentine network architecture bonded on the soft substrate (Ecoflex), with typical parameters including width $w_{PI/Cu}$ = 25 µm, thicknesses h_{Cu} = 0.5 µm, and h_{PI} = 24.5 µm, arc radius R = 500 µm, period length $\lambda_0 = 4R$, Young's moduli E_{Cu} = 124 GPa and

© 2022 Wiley-VCH GmbH

16163028, 2023, 7, Downloaded from https://onlinelibrary.wiley.com/doi/10.1002/adfm.202210880 by Institute Of Mechanics (Cas), Wiley Online Library on [08/05/2023]. See the Terms and Conditions (https://onlinelibrary.wiley.com/terms-and-conditions) on Wiley Online Library for rules of use; OA articles are governed by the applicable Creative Commons License

E_{PI} = 2.5 GPa, Poisson's ratio ν_{Cu} = 0.33 and ν_{PI} = 0.34 for the serpentine network, and thickness H = 50 µm, Young's modulus $E_{substrate}$ = 20 kPa[32,33] and Poisson's ratio $\nu_{substrate}$ = 0.49 for the soft substrate. The parameters of the skin include Young's modulus[59] E_{skin} = 2 MPa, Poisson's ratio ν_{skin} = 0.49 and thickness of 100 µm. The results with different Young's moduli of the skin and the soft substrate in Note S2 (Supporting Information) were also given.

Fabrication Processes of the Serpentine Structure: The fabrication processes of the serpentine structure were in the following. Step 1: A PI layer was spin-coated (2000 r.p.m. for 60 s) on a 4 µm thick constantan foil (Hanzhong Jingce, China) and cured at 250 °C for 4 h. The process was repeated 8 times to thicken the PI layer to 50 µm. A layer of 150 µm thick PI film was laminated on the 50 µm thick PI layer by resin adhesive. Step 2: The constantan layer was patterned to the off-axis serpentine structure by the standard photolithography process (including coating photoresist, pre-baking, UV exposure, development, corrosion of ferric chloride solution, and removal of photoresist). Step 3: The final serpentine structure was obtained after the pattern by an UV picosecond laser (DL566PU, DCT, China).

Stretching Tests of the Serpentine Structure: Stretching tests of the serpentine structure were carried out by a programmable tensile testing machine (ZQ-990A, ZHIQU, China). The resistance signals of the serpentine structure were measured by a digital multimeter (34461A, Keysight, USA).

Finite Element Analysis: The FEA was performed by employing the commercial software ABAQUS (SIMULIA, France). PI (Young's modulus = 2.5 GPa, Poisson's ratio = 0.34), Cu (Young's modulus = 124 GPa, Poisson's ratio = 0.33) and constantan (Young's modulus = 163 GPa, Poisson's ratio = 0.33) were all regarded as linear elastic materials. For relatively large deformation in Figure 4 and Figure S1 (Supporting Information), the material parameters of Ecoflex, which was regarded as a hyper elastic material described by the Mooney–Rivlin model, were C_{10} = 0.00805369 MPa, C_{01} = 0.00201342 MPa, and D_1 = 2 MPa^{-1}, respectively. For small deformation in Figure 2, Ecoflex was regarded as linear elastic material with Young's modulus = 62.3 kPa and Poisson's ratio = 0.49. In the FEA of the wavy-structure stretchable electronics, the number of uniform grids on the wave-like edge is one hundred and twenty, and one grid on other edges of the soft substrate is ≈0.3 h. In the FEA of the serpentine-structure stretchable electronics, the number of uniform grids along the line-width direction of the serpentine structure is twelve, and one grid of the serpentine structure along the neutral axis direction is ≈0.25w_{PI}; The in-plane grid size of the encapsulation is ≈0.25w_{PI}, and the number of uniform grids of the encapsulation along the thickness direction is sixteen. The hexahedron element C3D8RH was utilized for Ecoflex and the skin, and the shell element S4R for PI, Cu and constantan. The geometric configuration of the wave structure in the FEA is established as wavy-like in the initial state, rather than formed by buckling. To simulate the slidable interface in Figure 2b and Figure S1 (Supporting Information), a contact relationship is set between the bottom of the encapsulation layer and the skin in ABAQUS, that is, no separation in the normal direction and no friction in the tangential direction. Then the horizontal stretching is carried out at the left and right ends.

Supporting Information

Supporting Information is available from the Wiley Online Library or from the author.

Acknowledgements

Y.S. gratefully acknowledges the support from the National Natural Science Foundation of China (grant 12172359), Beijing Municipal Natural Science Foundation (no. 2202066), Key Research Program of Frontier Sciences of the Chinese Academy of Sciences (ZDBS-LY-JSC014), and CAS Interdisciplinary Innovation Team (JCTD-2020-03). The authors are also grateful to Yang Zhao and Maoyi Zhang for their technical support of the laser operation and software.

Conflict of Interest

The authors declare no conflict of interest.

Author Contributions

S.L. and Y.S. conceived the concept. S.L., Y.L. Y.H., Y.C., and Y.S. conducted the theoretical derivation, experimental fabrication and test, and discussed all the data. S.L. and Y.S. prepared the manuscript. Y.S. supervised the project.

Data Availability Statement

The data that support the findings of this study are available in the supplementary material of this article.

Keywords

consistency, design principle, interface conditions, stretchable inorganic electronics

Received: September 19, 2022
Revised: October 28, 2022
Published online: December 1, 2022

[1] D. H. Kim, J. L. Xiao, J. Z. Song, Y. G. Huang, J. A. Rogers, *Adv. Mater.* **2010**, *22*, 2108.
[2] J. A. Rogers, T. Someya, Y. G. Huang, *Science* **2010**, *327*, 1603.
[3] Z. G. Xue, H. L. Song, J. A. Rogers, Y. H. Zhang, Y. G. Huang, *Adv. Mater.* **2020**, *32*, 1902254.
[4] S. Xu, Y. H. Zhang, J. Cho, J. Lee, X. Huang, L. Jia, J. A. Fan, Y. W. Su, J. Su, H. G. Zhang, H. Y. Cheng, B. W. Lu, C. J. Yu, C. Chuang, T. I. Kim, T. Song, K. Shigeta, S. Kang, C. Dagdeviren, I. Petrov, P. V. Braun, Y. G. Huang, U. Paik, J. A. Rogers, *Nat. Commun.* **2013**, *4*, 1543.
[5] L. Z. Xu, S. R. Gutbrod, A. P. Bonifas, Y. W. Su, M. S. Sulkin, N. S. Lu, H. J. Chung, K. I. Jang, Z. J. Liu, M. Ying, C. Lu, R. C. Webb, J. S. Kim, J. I. Laughner, H. Y. Cheng, Y. H. Liu, A. Ameen, J. W. Jeong, G. T. Kim, Y. G. Huang, I. R. Efimov, J. A. Rogers, *Nat. Commun.* **2014**, *5*, 3329.
[6] X. L. Hu, P. Krull, B. de Graff, K. Dowling, J. A. Rogers, W. J. Arora, *Adv. Mater.* **2011**, *23*, 2933.
[7] Y. W. Su, X. C. Ping, K. J. Yu, J. W. Lee, J. A. Fan, B. Wang, M. Li, R. Li, D. V. Harburg, Y. A. Huang, C. J. Yu, S. M. Mao, J. Shim, Q. L. Yang, P. Y. Lee, A. Armonas, K. J. Choi, Y. C. Yang, U. Paik, T. Chang, T. J. Dawidczyk, Y. G. Huang, S. D. Wang, J. A. Rogers, *Adv. Mater.* **2017**, *29*, 1604989.
[8] Y. Y. Yang, M. Z. Wu, A. Vazquez-Guardado, A. J. Wegener, J. G. Grajales-Reyes, Y. J. Deng, T. Y. Wang, R. Avila, J. A. Moreno, S. Minkowicz, V. Dumrongprechachan, J. Lee, S. Y. Zhang, A. A. Legaria, Y. H. Ma, S. Mehta, D. Franklin, L. Hartmann, W. B. Bai, M. D. Han, H. B. Zhao, W. Lu, Y. Yu, X. Sheng, A. Banks, X. G. Yu, Z. R. Donaldson, R. W. Gereau, C. H. Good, Z. Q. Xie, et al., *Nat. Neurosci.* **2021**, *24*, 1035.

 © 2022 Wiley-VCH GmbH

16163028, 2023, 7, Downloaded from https://onlinelibrary.wiley.com/doi/10.1002/adfm.202210880 by Institute Of Mechanics (Cas), Wiley Online Library on [08/05/2023]. See the Terms and Conditions (https://onlinelibrary.wiley.com/terms-and-conditions) on Wiley Online Library for rules of use; OA articles are governed by the applicable Creative Commons License

[9] S. Li, G. D. Liu, R. Li, Q. L. Li, Y. Zhao, M. Q. Huang, M. Y. Zhang, S. Z. Yin, Y. X. Zhou, H. Tang, L. W. Wang, G. H. Fang, Y. W. Su, *ACS Nano* **2022**, *16*, 541.
[10] D. H. Kim, N. S. Lu, R. Ma, Y. S. Kim, R. H. Kim, S. D. Wang, J. Wu, S. M. Won, H. Tao, A. Islam, K. J. Yu, T. I. Kim, R. Chowdhury, M. Ying, L. Z. Xu, M. Li, H. J. Chung, H. Keum, M. McCormick, P. Liu, Y. W. Zhang, F. G. Omenetto, Y. G. Huang, T. Coleman, J. A. Rogers, *Science* **2011**, *333*, 838.
[11] D. Y. Khang, H. Q. Jiang, Y. Huang, J. A. Rogers, *Science* **2006**, *311*, 208.
[12] D. H. Kim, J. H. Ahn, W. M. Choi, H. S. Kim, T. H. Kim, J. Z. Song, Y. G. Y. Huang, Z. J. Liu, C. Lu, J. A. Rogers, *Science* **2008**, *320*, 507.
[13] Y. G. Sun, W. M. Choi, H. Q. Jiang, Y. G. Y. Huang, J. A. Rogers, *Nat. Nanotechnol.* **2006**, *1*, 201.
[14] M. D. Han, L. Chen, K. Aras, C. M. Liang, X. X. Chen, H. B. Zhao, K. Li, N. R. Faye, B. H. Sun, J. H. Kim, W. B. Bai, Q. S. Yang, Y. H. Ma, W. Lu, E. M. Song, J. M. Baek, Y. J. Lee, C. Liu, J. B. Model, G. J. Yang, R. Ghaffari, Y. G. Huang, I. R. Efimov, J. A. Rogers, *Nat. Biomed. Eng.* **2020**, *4*, 997.
[15] R. Li, M. Li, Y. W. Su, J. Z. Song, X. Q. Ni, *Soft Matter* **2013**, *9*, 8476.
[16] Y. W. Su, J. Wu, Z. C. Fan, K. C. Hwang, J. Z. Song, Y. G. Huang, J. A. Rogers, *J Mech Phys Solids* **2012**, *60*, 487.
[17] H. C. Ko, M. P. Stoykovich, J. Z. Song, V. Malyarchuk, W. M. Choi, C. J. Yu, J. B. Geddes, J. L. Xiao, S. D. Wang, Y. G. Huang, J. A. Rogers, *Nature* **2008**, *454*, 748.
[18] D. H. Kim, J. Z. Song, W. M. Choi, H. S. Kim, R. H. Kim, Z. J. Liu, Y. Y. Huang, K. C. Hwang, Y. W. Zhang, J. A. Rogers, *Proc. Natl. Acad. Sci. USA* **2008**, *105*, 18675.
[19] J. Song, Y. Huang, J. Xiao, S. Wang, K. C. Hwang, H. C. Ko, D. H. Kim, M. P. Stoykovich, J. A. Rogers, *J. Appl. Phys.* **2009**, *105*, 123516.
[20] S. D. Wang, J. L. Xiao, J. Z. Song, H. C. Ko, K. C. Hwang, Y. G. Huang, J. A. Rogers, *Soft Matter* **2010**, *6*, 5757.
[21] T. S. Pan, M. Pharr, Y. J. Ma, R. Ning, Z. Yan, R. X. Xu, X. Feng, Y. G. Huang, J. A. Rogers, *Adv. Funct. Mater.* **2017**, *27*, 1702589.
[22] Y. H. Zhang, S. D. Wang, X. T. Li, J. A. Fan, S. Xu, Y. M. Song, K. J. Choi, W. H. Yeo, W. Lee, S. N. Nazaar, B. W. Lu, L. Yin, K. C. Hwang, J. A. Rogers, Y. G. Huang, *Adv. Funct. Mater.* **2014**, *24*, 2028.
[23] T. Widlund, S. X. Yang, Y. Y. Hsu, N. S. Lu, *Int. J. Solids Struct.* **2014**, *51*, 4026.
[24] S. X. Yang, S. T. Qiao, N. S. Lu, *J. Appl. Mech-T Asme.* **2017**, *84*, 021004.
[25] Y. H. Zhang, H. R. Fu, Y. W. Su, S. Xu, H. Y. Cheng, J. A. Fan, K. C. Hwang, J. A. Rogers, Y. G. Huang, *Acta Mater.* **2013**, *61*, 7816.
[26] Y. H. Zhang, S. Xu, H. R. Fu, J. Lee, J. Su, K. C. Hwang, J. A. Rogers, Y. G. Huang, *Soft Matter* **2013**, *9*, 8062.
[27] K. Huang, R. Dinyari, G. Lanzara, J. Y. Kim, J. M. Feng, C. Vancura, F. K. Chang, P. Peumans, *2007 IEEE International Electron Devices Meeting*, **2007**, pp. 217–220, https://doi.org/10.1109/IEDM.2007.4418906.
[28] C. Lv, H. Yu, H. Jiang, *Extreme Mech. Lett.* **2014**, *1*, 29.
[29] M. U. Rehman, J. P. Rojas, *Extreme Mech. Lett.* **2017**, *15*, 44.
[30] J. P. Rojas, A. Arevalo, I. G. Foulds, M. M. Hussain, *Appl. Phys. Lett.* **2014**, *105*, 154101.
[31] W. L. Sung, C. C. Chen, K. Huang, W. Fang, *J. Micromech. Microeng.* **2016**, *26*, 025003.
[32] K. Li, X. Cheng, F. Zhu, L. Z. Li, Z. Q. Xie, H. W. Luan, Z. H. Wang, Z. Y. Ji, H. L. Wang, F. Liu, Y. G. Xue, C. Q. Jiang, X. Feng, L. M. Li, J. A. Rogers, Y. G. Huang, Y. H. Zhang, *Adv. Funct. Mater.* **2019**, *29*, 1806630.
[33] K. I. Jang, K. Li, H. U. Chung, S. Xu, H. N. Jung, Y. Y. Yang, J. W. Kwak, H. H. Jung, J. Song, C. Yang, A. Wang, Z. J. Liu, J. Y. Lee, B. H. Kim, J. H. Kim, J. Lee, Y. Yu, B. J. Kim, H. Jang, K. J. Yu, J. Kim, J. W. Lee, J. W. Jeong, Y. M. Song, Y. G. Huang, Y. H. Zhang, J. A. Rogers, *Nat. Commun.* **2017**, *8*, 15894.
[34] Y. Liu, Z. Yan, Q. Lin, X. L. Guo, M. D. Han, K. Nan, K. C. Hwang, Y. G. Huang, Y. H. Zhang, J. A. Rogers, *Adv. Funct. Mater.* **2016**, *26*, 2909.
[35] S. Xu, Z. Yan, K. I. Jang, W. Huang, H. R. Fu, J. Kim, Z. Wei, M. Flavin, J. McCracken, R. Wang, A. Badea, Y. Liu, D. Q. Xiao, G. Y. Zhou, J. Lee, H. U. Chung, H. Y. Cheng, W. Ren, A. Banks, X. L. Li, U. Paik, R. G. Nuzzo, Y. G. Huang, Y. H. Zhang, J. A. Rogers, *Science* **2015**, *347*, 154.
[36] J. A. Fan, W. H. Yeo, Y. W. Su, Y. Hattori, W. Lee, S. Y. Jung, Y. H. Zhang, Z. J. Liu, H. Y. Cheng, L. Falgout, M. Bajema, T. Coleman, D. Gregoire, R. J. Larsen, Y. G. Huang, J. A. Rogers, *Nat. Commun.* **2014**, *5*, 3266.
[37] Q. Ma, Y. H. Zhang, *J. Appl. Mech-T Asme* **2016**, *83*, 111008.
[38] J. J. S. Norton, D. S. Lee, J. W. Lee, W. Lee, O. Kwon, P. Won, S. Y. Jung, H. Y. Cheng, J. W. Jeong, A. Akce, S. Umunna, I. Na, Y. H. Kwon, X. Q. Wang, Z. J. Liu, U. Paik, Y. G. Huang, T. Bretl, W. H. Yeo, J. A. Rogers, *Proc. Natl. Acad. Sci. USA* **2015**, *112*, 3920.
[39] Y. W. Su, S. D. Wang, Y. A. Huang, H. W. Luan, W. T. Dong, J. A. Fan, Q. L. Yang, J. A. Rogers, Y. G. Huang, *Small* **2015**, *11*, 367.
[40] L. Z. Xu, S. R. Gutbrod, Y. J. Ma, A. Petrossians, Y. H. Liu, R. C. Webb, J. A. Fan, Z. J. Yang, R. X. Xu, J. J. Whalen, J. D. Weiland, Y. G. Huang, I. R. Efimov, J. A. Rogers, *Adv. Mater.* **2015**, *27*, 1731.
[41] Y. H. Zhang, H. R. Fu, S. Xu, J. A. Fan, K. C. Hwang, J. Q. Jiang, J. A. Rogers, Y. G. Huang, *J Mech Phys Solids* **2014**, *72*, 115.
[42] M. K. Blees, A. W. Barnard, P. A. Rose, S. P. Roberts, K. L. McGill, P. Y. Huang, A. R. Ruyack, J. W. Kevek, B. Kobrin, D. A. Muller, P. L. McEuen, *Nature* **2015**, *524*, 204.
[43] Y. Cho, J. H. Shin, A. Costa, T. A. Kim, V. Kunin, J. Li, S. Y. Lee, S. Yang, H. N. Han, I. S. Choi, D. J. Srolovitz, *Proc. Natl. Acad. Sci. USA* **2014**, *111*, 17390.
[44] A. Lamoureux, K. Lee, M. Shlian, S. R. Forrest, M. Shtein, *Nat. Commun.* **2015**, *6*, 8092.
[45] A. Rafsanjani, K. Bertoldi, *Phys. Rev. Lett.* **2017**, *118*, 084301.
[46] T. C. Shyu, P. F. Damasceno, P. M. Dodd, A. Lamoureux, L. Z. Xu, M. Shlian, M. Shtein, S. C. Glotzer, N. A. Kotov, *Nat. Mater.* **2015**, *14*, 785.
[47] Y. C. Tang, G. J. Lin, S. Yang, Y. K. Yi, R. D. Kamien, J. Yin, *Adv. Mater.* **2017**, *29*, 1604262.
[48] L. Z. Xu, T. C. Shyu, N. A. Kotov, *ACS Nano* **2017**, *11*, 7587.
[49] S. Timoshenko, J. N. Goodier, *Theory of Elasticity*, McGraw-Hill, New York **1969**.
[50] C. O. Horgan, J. K. Knowles, *Adv. Appl. Mech.* **1983**, *23*, 179.
[51] E. Sternberg, *Q Appl Math* **1954**, *11*, 393.
[52] R. Vonmises, *B Am Math Soc.* **1945**, *51*, 555.
[53] E. Cerda, L. Mahadevan, *Phys. Rev. Lett.* **2003**, *90*, 074302.
[54] X. Chen, J. W. Hutchinson, *J. Appl. Mech-T Asme* **2004**, *71*, 597.
[55] Z. Y. Huang, W. Hong, Z. Suo, *J Mech Phys Solids* **2005**, *53*, 2101.
[56] H. F. Li, S. S. Cai, Y. C. Zhang, K. C. Hwang, Y. J. Ma, X. Feng, *Extreme Mech. Lett.* **2019**, *29*, 100453.
[57] Y. P. Liu, K. Guo, C. G. Wang, H. J. Gao, *J Mech Phys Solids* **2019**, *123*, 103.
[58] B. Li, Y.-P. Cao, X.-Q. Feng, H. Gao, *Soft Matter* **2012**, *8*, 5728.
[59] M. Geerligs, L. van Breemen, G. Peters, P. Ackermans, F. Baaijens, C. Oomens, *J. Biomech.* **2011**, *44*, 1176.

© 2022 Wiley-VCH GmbH

16163028, 2023, 7, Downloaded from https://onlinelibrary.wiley.com/doi/10.1002/adfm.202210880 by Institute Of Mechanics (Cas), Wiley Online Library on [08/05/2023]. See the Terms and Conditions (https://onlinelibrary.wiley.com/terms-and-conditions) on Wiley Online Library for rules of use; OA articles are governed by the applicable Creative Commons License